Integrated HF CMOS-MEMS Square-Frame Resonators
with On-Chip Electronics and Electrothermal Narrow Gap Mechanism

Chiung-Cheng Lo[1], Fang Chen[1], and G.K. Fedder[1,2]
[1]Department of Electrical and Computer Engineering and [2]The Robotics Institute
Carnegie Mellon University, Pittsburgh, PA, 15213, USA
Email: chiungcl@ece.cmu.edu Tel: 412-268-6606. Fax: 412-268-4594

ABSTRACT

A fully differential square frame resonator (SFR), operating at resonant frequencies of 6.184MHz and 17.63MHz for the fundamental and 2nd harmonic, respectively, is introduced, which is the highest resonant frequency reported to date in CMOS-MEMS technology. In-plane CMOS-MEMS resonators have been fabricated directly on a conventional CMOS substrate with on-chip differential amplifiers. To enhance the output motional current, an electrothermal-actuated electrode is designed to reduce the input/output capacitive gap. A 5μm-thick, 4 μm-wide, 63 μm-long SFR with fixed electrodes exhibits a quality factor of 996 in vacuum at 6.18MHz.
Keywords: Integrated resonator, CMOS-MEMS, HF, RF MEMS

1. INTRODUCTION

The reliance on off-chip resonators and filters in superheterodyne front-end architectures limits the miniaturization of portable communication devices. Ever since micromachined resonators were introduced, the signal processing application as a bandpass filter has been graining considerable attention in order to reduce the filter size and to integrate resonators on-chip [1]. Recent developments in MEMS technologies offer high quality factor (Q) and high operational frequency. For example, hollow-disk ring resonators have been demonstrated with Q> 60,000 at 24 MHz and Q>14,000 at 1.2GHz [2]. By mechanical or electrostatic coupling, MEMS resonators yield filtering and mixing functions with miniature size [3]-[6].

This work introduces a square-frame resonator that consists of four free-free beams connected at the nodal points of the first flexural resonant mode. The design greatly provides large output currents and removes the issue of frequency mismatch [7]. This work differs from previous CMOS MEMS resonators by having higher working frequency and inherent differential operation. Integrated with custom-designed CMOS circuits, micromechanical resonators are fabricated using a conventional 0.35-μm CMOS process followed by post-
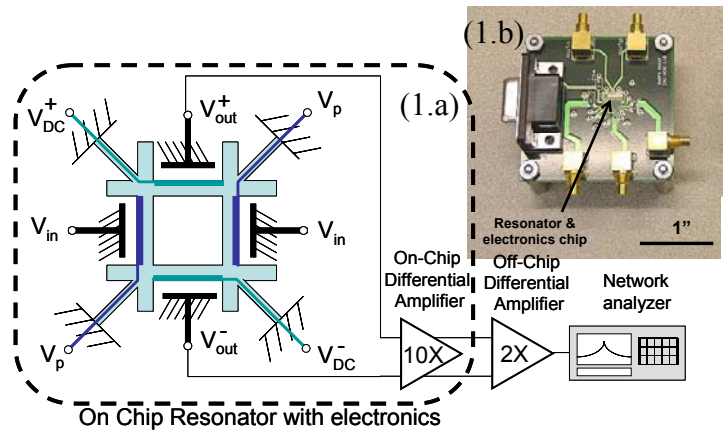

Figure 1 (a) The schematic of SFR in a two-port bias and excitation configuration. **(b)** The test bench of micromechanical resonator.

CMOS dielectric layer etching and silicon etching for structural release. To reduce the motional resistance, sub-micron gaps are necessary on the input and output between the resonator and the stator electrodes. By implementing CMOS-MEMS electrothermal-actuated electrodes, a sub-micron-wide capacitive gap can be achieved. This paper details the design and fabrication principles that allow CMOS MEMS technology to achieve high operating frequency and greatly improved performance needed for potentially use in wireless communication receivers.

2. ENLARGING MOTIONAL CURRENT

The motional current is given by:

$$i_{out} = (V_{out} - V_{dc}) \times \frac{\varepsilon_0 \cdot A \cdot \omega \cdot x}{(g-x)^2} \qquad (1)$$

where V_{out} and V_{dc} are the voltages applied at the output electrodes, and x, g, and A are the mechanical displacement, electrode gap distance and electrode size, respectively. One approach to attain the high motional current is to increase the electrode size. However, this approach often increases the mass of the resonator and leads to an undesired lowering of the resonant frequency. Another approach to increase motional current is to
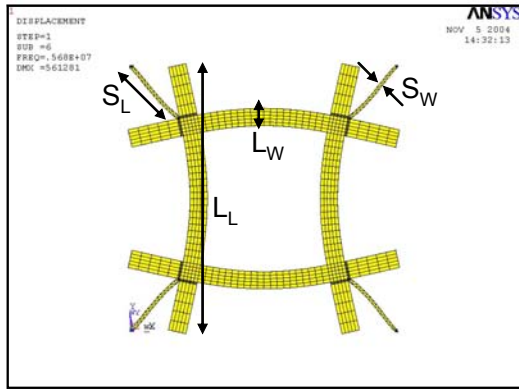
Figure 2 Finite element simulation of 1st flexural free-free mode with critical dimension (5.67 MHz)
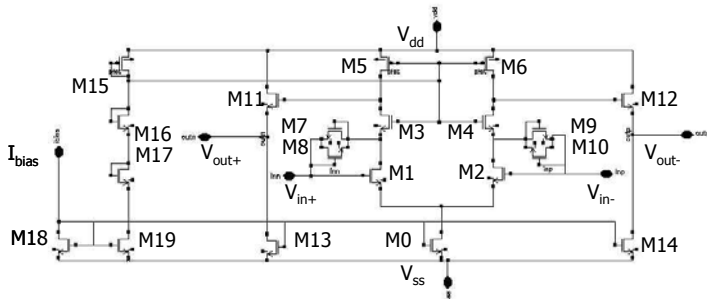

Figure 3 The schematic of on chip differential amplifier with 5mW power consumption.

Table 1: Square frame resonator design summary

Parameters	Design	Measurement	Unit
Resonator Beam Length, L_L	63	64.7	µm
Resonator Beam Width, L_W	4	4.63	µm
Support Beam Length, S_L	6.3	6.35	µm
Structure Thickness, S_W	5	-	µm
Fixed Gap distance	0.9	0.87	µm
Polarization Voltage, V_p	-	5	Volts
DC-Bias Voltage, V_{DC}	-	20	Volts
Resonant Frequency, 1st mode	5.67	6.184	MHz
Resonant Frequency, 2nd mode	17.31	17.63	MHz

implement an array of identical parallel resonators, and then to augment the signal by connecting all output electrodes together, which obviates the problem of lowering frequency. However, this requires a resonant-frequency tuning mechanism to ensure all devices vibrate synchronously.

The schematic of the integrated CMOS-MEMS SFR and test board is shown in Fig. 1. The resonator consists of four free-free beams suspended at their nodal points by four quarter-wavelength-long support beams for

minimum energy loss. A 0.9-µm-wide capacitive gap is established. The fixed 20 µm-long, 5 µm-thick electrodes associated with the input gap are connected to the input signal, V_{in}, and the resonator electrodes are connected to the polarization voltage, V_p. The resulting electrostatic force actuates the SFR at the desired resonant frequency. Finite element analysis of the fundamental resonant mode shape is illustrated in Fig. 2. DC bias voltages, $\pm V_{DC}$, are connected to the inner movable output electrodes, creating a differential displacement current through the time-varying capacitance. The output electrodes are wired into an on-chip differential amplifier with DC self-biasing at ~1.3V, shown in Fig. 3. With 5mW power consumption (V_{dd}=5V and I_{bias}=0.2mA), the on-chip amplifier converts the motional current to a voltage through its input capacitance with an effective voltage gain of 10. The output voltage is further amplified by an off-chip amplifier, and then measured with a network analyzer. Table 1, along with Fig. 2 summaries the geometric sizing of the SFR.
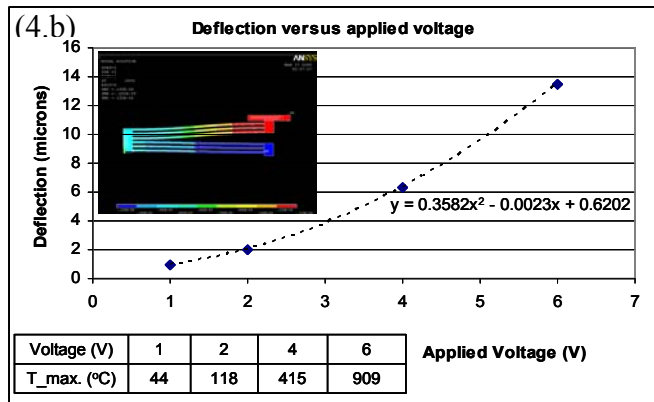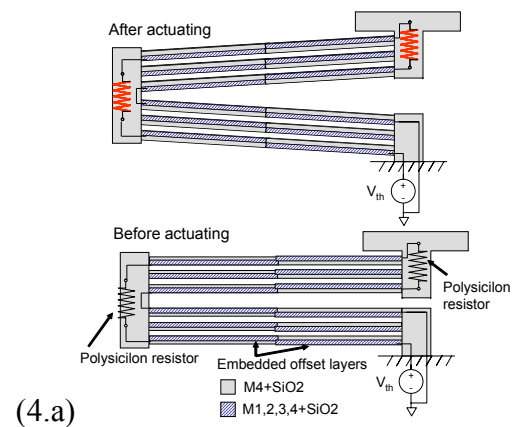

(4.a)

(4.b)

Voltage (V)	1	2	4	6
T_max. (ºC)	44	118	415	909

Figure 4 (a) The mechanism of CMOS-MEMS electrothermal actuator. (b) The simulated deflection versus supplied voltage of the actuator.

3. MECHANISM OF NARROW GAP

In order to lower the motional resistance and termination impedance, a narrow electrode gap is desired. To date, the narrowest gap that has been achieved is around a few hundred angstroms [2], which leads to motional resistance approaching 50Ω. However, the fabrication process of such device is not compatible with conventional CMOS steps as the process temperatures are as high as 920°C, which is not suitable for post CMOS steps.

Sub-micron gaps can be achieved by implementing a CMOS-MEMS electrothermal actuator to narrow the gap after fabrication is completed [8]. As illustrated in Fig. 4(a), the actuator comprises of two adjacent stacks of layers having different thermal expansion rates. By employing a polysilicon heating resistor within the actuator and supplying DC current, the localized high temperature creates an internal bending moment that moves the device laterally. The simulated deflection is shown in Fig 4(b). The final gap is defined by the difference between the initial gap as designed and the gap to the limit stop. The minimum gap, estimated around 25 nm, is limited by the mask resolution and the tolerances of lithography and etching processes.

4. CMOS-MEMS FABRICATION

As illustrated in Fig. 5(a), the post CMOS micromachining process [9] starts with a foundry-fabricated four-metal CMOS chip. A $CHF_3:O_2$ reactive-ion etch (RIE) of the intermetal dielectric stack removes all dielectric not covered by top metal layers as shown in Fig. 5(b). The choice of the top most metal layer determines the structure thickness. Under the protection of the top metal, other metal layers can be used for routing electrical signals and for shielding. After the dielectric etch, a timed directional deep-RIE of the exposed silicon substrate dictates the depth of the silicon pit underneath the device. This step is followed by a timed isotropic silicon etch in an SF_6 plasma to undercut and release the structure, resulting in Fig. 5(c).
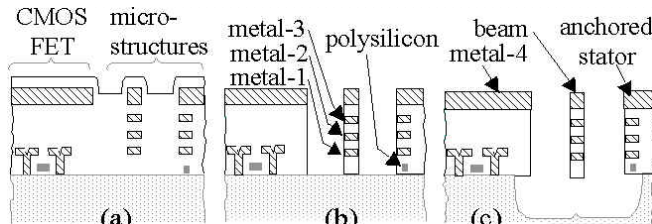

Figure 5 Cross-section of CMOS micromachining process [9]; (a) after foundry CMOS processing, (b) after anisotropic etch, (c) after release the structure by DRIE etch.

5. MEASUREMENT RESULTS

The SEM of a 5 μm-thick, 4 μm-wide, 63 μm-long SFR with a 0.9 μm-wide electrode-to-resonator gap is shown in Fig. 6. Despite of the motional impedance being much larger than 50Ω, fabricated devices in the 1 to 10 MHz range were still measurable in a direct two-
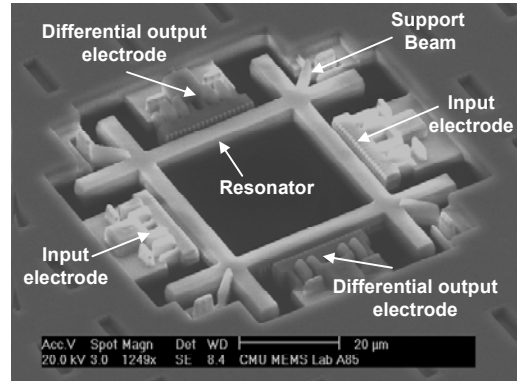

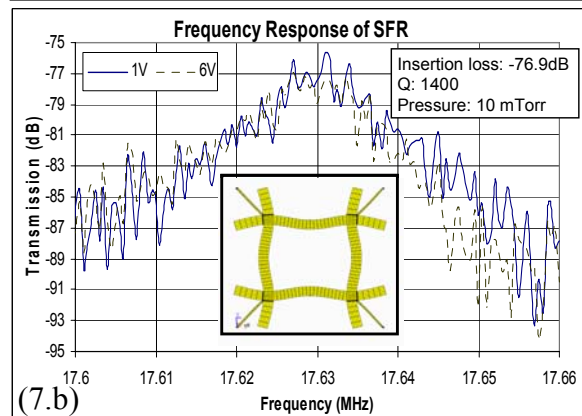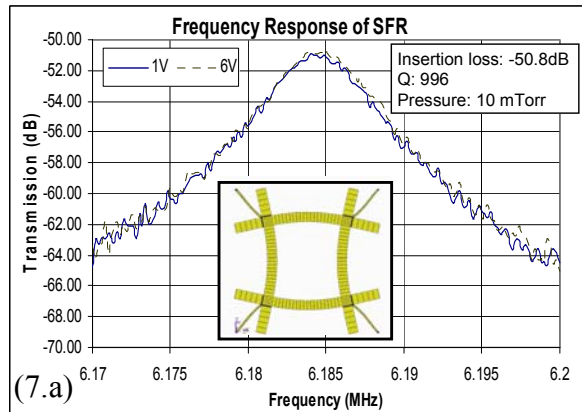**Figure 6** The SEM of HF CMOS MEMS square frame resonator.

Figure 7 Measured frequency characteristics with different V_p for (a) 1st mode and (b) 2nd mode
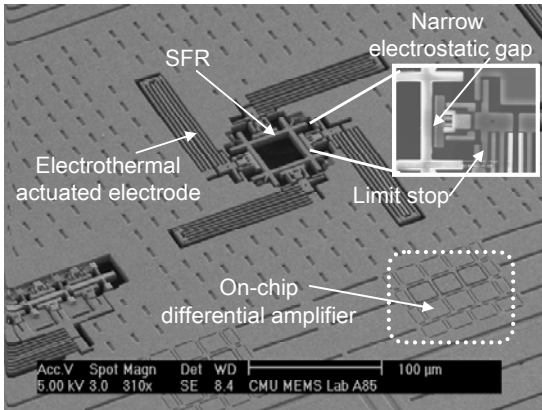
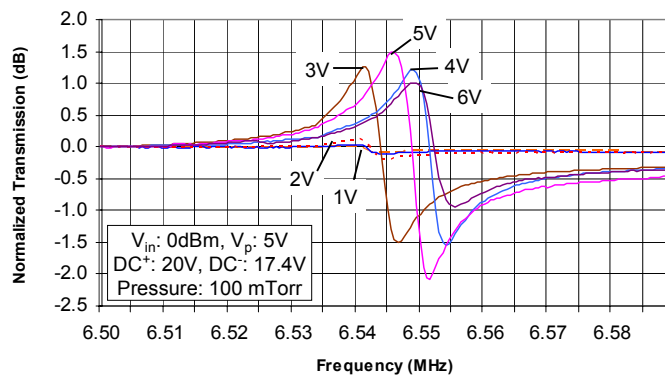**Figure 8** The SEM of SFR with electrothermal actuated electrodes.

Figure 9 Measured frequency response of SFR with different thermal-actuated voltages for 1st resonant mode.

port configuration using a network analyzer. After subtracting the feedthrough disturbance due to parasitic capacitance, the frequency responses of the two lowest lateral modes are obtained and shown in Fig. 7(a)-(b).

The operating conditions are V_{in}=0 dBm, V_{DC+}=20V and V_{DC-}=17.4V, which set the DC voltage across the output gaps to ±18.7V. The measured frequency responses represent the vibration at fundamental and 2nd flexural free-free mode with center frequency values of 6.184MHz and 17.63MHz, Q of 996 and 1400, and insertion loss of 50.8dB and 76.96dB, respectively.

Another SFR of identical size was designed with electrothermally actuated electrodes, as shown in the SEM in Fig. 8. Without subtracting the feedthrough disturbance, but normalizing it to initial measured points for easy comparison of different actuation voltages, the frequency response in Fig. 9 was obtained. The transmission gain increases with increasing the actuation heater voltage from 1V to 3V. However, this tendency does not hold for the actuation voltages higher than 4V. From the simulation result, the highest temperature of the electrothermal actuator is over 400°C, for 4V operation,

and around 900°C for 6V operation. This high temperature is believed to have caused the device to melt partially and deform the limit stop resulting in lowering resonant frequency for 5V than that of 4V in Fig. 9.

6. CONCLUSION

We have presented a fully differential square frame resonator (SFR), operating at a resonant frequency of 6.184MHz and 17.63MHz for the fundamental and 2nd harmonic modes, respectively, which is the highest filter frequency to date achieved in CMOS-MEMS technology. The implementation of the differential output in a single micromechanical resonator eliminates the issue of frequency mismatch to improve common-mode noise rejection. To enhance the electrical motional current, an electrothermal-actuated electrode is designed to reduce the input/output capacitive gap. Future CMOS-MEMS resonators should exploit self-assembly characteristics of these actuators to achieve down to 25 nm gaps without the need for actuator power. To work as a viable filter, future work must focus on identification and reduction of direct capacitive feedthrough present in the transmission characteristics.

REFERENCE

[1] L. Lin, C.-T.C. Nguyen, R.T. Howe, and A.P. Pisano, "Micro electromechanical filters for signal processing," *IEEE MEMS Workshop*, pp.226-231, Feb. 1992.

[2] S.-S. Li, Y.-Q. Lin, Y.Xie, Z. Ren, and C.T.-C. Nguyen, "Micromechanical hollow-disk ring resonators," *MEMS '04*, pp.821-824

[3] A. Wong, and C.-T.C. Nguyen, "Micromechanical mixer-filters*," J. Microelectromechanical System*. vol. 13, no. 1, 2004, pp.100-112.

[4] S. Pourkamali, R.Abdolvand, and F. Ayazi, "A 600 kHz electrically-coupled MEMS bandpass filter," *MEMS'03*, pp. 702 – 705.

[5] L. Lin, R.T. Howe, and A.P. Pisano, "Micro-electromechanical filters for signal processing**," J. Microelectromechanical Systems*, V. 7, 1998 pp. 286 – 294

[6] D. Galayko, A. Kaiser, L. Buchaillot, D. Collard,and C. Combi, "Electrostatical coupling-spring for micro-mechanical filtering applications," *ISCAS '03*, vol.3, pp. 530-533.

[7] F. Chen, J. Brotz, U. Arslan, C.C. Lo, T. Mukherjee, and G.K. Fedder, "CMOS-MEMS Resonant RF Mixer-Filters," *MEMS'05*, pp. 24-27

[8] A. Oz, and G.K. Fedder, "CMOS/BiCMOS Self-Assembling and Electrothermal Microactuators for Tunable Capacitors Gap-closing Structures and Latch Mechanisms," *2004 Solid-State Sensor, Actuator and Microsystems Workshop, Hilton Head* Is., SC, pp. 212-215.

[9] G.K. Fedder, S. Santhanam, M.L. Reed, S.C. Eagle, D.F. Guillou, M.S.-C. Lu, and L.R. Carley, "Laminated High-Aspect-ratio Microstructures in a Conventional CMOS Process*," Sensors & Actuators*, March 1997, pp. 103-110.